J. Fluid Mech. (1997), *vol.* 335, *pp.* 393–413

Normal modes of an ice sheet

By RICHARD C. A. HINDMARSH

British Antarctic Survey, Natural Environment Research Council, High Cross, Madingley Road, Cambridge CB3 0ET, UK

(Received 14 June 1995 and in revised form 1 November 1996)

A linearized perturbation about the Vialov–Nye fixed-span solution for a steady-state ice sheet yields a Sturm-Liouville problem. The numerical eigenvalue problem is solved and the resulting normal modes are used to compute Green's and influence functions for perturbations to the accumulation rate, the rate factor and for long-wavelength basal topography. The eigenvalue for the slowest mode is approximately the same as that predicted by the zero-dimensional theory. It is found that the sensitivity of the steady profile to accumulation is greatest in the central area of the ice sheet, while the sensitivity to rate factor is greatest near the margin. The antisymmetric perturbation provides information about the relaxation time for divide motion and spatial variation in the sensitivity of divide deviation from the ice-sheet centre to accumulation rate variations. The use of the method for model initialization is considered. Forcing deviations of 30% give relative errors in the perturbation of about 10%.

1. Introduction

The nonlinearity in ice-sheet flows often acts to make ice sheets insensitive to changes in the controlling parameters: for example, a two-fold increase in the accumulation rate will only increase the steady thickness of the ice by a factor of $2^{1/8} \approx 1.09$ (e.g. Hindmarsh 1990). The small changes involved in short-term behaviour, for example the response to global change, are describable by linear theory, which permits a broad range of techniques to be used in analysing ice sheet response and in data assimilation. Scale model applications of these principles can be found in Oerlemans (1981) and Van der Veen (1993).

Our main concern will be with computing the normal modes to a perturbation around the Vialov–Nye (VN) steady-state equation for an ice-sheet profile (Vialov 1958; Nye 1959). This solution has its limitations and has had criticism (Nagata 1977; Hutter 1983) owing to its non-physical margin condition, but yields a considerable simplification by fixing the margin position. The normal modes allow us to compute Green's functions or more general influence functions which analyse the spatial variability of the sensitivity of the steady profile at a given point to forcing imposed at any given point, as well as being a convenient technique for data assimilation through normal-mode initialization techniques. The analysis in this paper has been used in an investigation into the stochastic behaviour of divide position (Hindmarsh 1996).

Linearizations of the evolution equations for ice-sheet thickness have been reviewed by Hutter (1983, chap. 6). Two pre-computer glaciological examples are Bodvarsson (1955) and Nye (1959). Both of these can be criticised (e.g. Fowler 1992)

for not considering the boundary condition at the margin properly. Linearizations have also been carried out by Halfar (1981), Hindmarsh (1990) and Fowler (1992), but the analysis presented here is the first consistent treatment of symmetric and antisymmetric perturbations for a nonlinear rheology.

2. Mathematical development

2.1. *The ice-sheet equation*

The governing equation derived below is the ice-sheet equation

$$\partial_t H = \frac{1}{\omega(x)} \partial_x \left(\omega(x) C H^m |\partial_x s|^{v-1} \partial_x s \right) + a, \tag{2.1}$$

where we are considering a coordinate system (x, z, t). Only plane and axisymmetric configurations are considered. Here, $H(x,t)$ is the thickness of the ice sheet, $s(x,t)$ is the upper surface, $\omega(x)$ is the flow-line width and $a(x,t)$ is the surface mass-balance exchange. This particular equation describes the evolution of ice-sheet thickness where the flow mechanism is either internal deformation according to some nonlinearly viscous flow power law or sliding according to some Weertman-type law. Normal-mode analyses are not however limited to these situations.

Various boundary conditions can be applied to the ice-sheet equation, but we shall consider the VN fixed-span/finite-flux boundary conditions. The field equation (2.1) is solved on a domain $x \in [-S, S]$ with boundary conditions $H(\pm S) \equiv 0$. Physically, this can be considered as an ice sheet which has expanded to the continental margin.

The quantity C is directly related to either a weighted vertical average rate factor $\bar{A}_d$ defined below in (2.3) of the rate factor A_d used in the viscous relationship

$$E = A_d \tau^n,$$

where E is a second invariant of the deformation rate and τ is a second invariant of the deviator stress (Glen 1955) or comes from a sliding relation of the form

$$u_b = A_s \tau_b^{\ell}.$$

We construct the following quantities for use in the general evolution equation:

$$v = \begin{cases} n \\ \ell \end{cases}, \qquad m = \begin{cases} n+2 \\ \ell+1 \end{cases}, \qquad C = \begin{cases} [2/(n+2)]\bar{A}_d & \text{internal deformation} \\ A_s & \text{sliding.} \end{cases}$$

We sketch the now standard (Hutter 1983; Morland 1984; Fowler 1992) derivation of equation (2.1) using the shallow ice approximation. Vertical distances are scaled by thickness magnitude $[H]$, horizontal distances by span magnitude $[S]$, accumulation rates by $[a]$, time by $[t] = [H]/[a]$ and rate factor $[C]$ by $[C] = [a][S]^{v+1}/[\rho]^v [g]^v [H]^{m+v}$ where $[\rho], [g]$ are the magnitude of the density of ice and the acceleration due to gravity. The magnitude of the shear stress $[\tau_{xz}]$ is

$$[\tau_{xz}] = \frac{[\rho][g][H]^2}{[S]} = \epsilon[\rho][g][H] = \epsilon[p], \ \epsilon = \frac{[H]}{[S]} \ll 1$$

where ϵ is the aspect ratio of the problem and $[p]$ is the pressure magnitude.

The shallow ice approximation expands the Stokes equations in terms of the aspect ratio, treating it as a global parameter representing deviation from static conditions.

The quasi-static formula for the shear stress introduced into glaciology by Nye (1952), $\tau_{xz} = -\rho g(s-z)\partial_x s$, is re-obtained as the asymptotic approximation

$$\tau_{xz} = -\rho g(s-z)\partial_x s + O\left(\epsilon^2\right), \tag{2.2}$$

and the shallow ice approximation also yields

$$\tau \simeq |\tau_{xz}|\,;\; E \simeq \tfrac{1}{2}\partial_z u;\; \partial_z u = 2A\,|\tau_{xz}|^{v-1}\,\tau_{xz}.$$

When internal deformation is being considered, substitution of the approximate relationship (2.2) and two integrations with respect to z yield a formula for the ice flux

$$q = -\frac{2\bar{A}_d}{v+2}H^m\,|\partial_x s|^{v-1}\,\partial_x s, \quad \bar{A}_d = (n+2)\int_0^1 (1-\zeta)^{n+1}\,A_d \mathrm{d}\zeta, \tag{2.3}$$

where $\zeta = (z-b)/H$. If we are treating sliding, then we simply write $q = u_b H = -A_s H^m\,|\partial_x s|^{\ell-1}\,\partial_x s$, and we may write a general flux formula

$$q = -CH^m\,|\partial_x s|^{v-1}\,\partial_x s, \tag{2.4}$$

which, when used with the continuity equation

$$\partial_t H + \frac{1}{\omega}\partial_x(\omega q) = a, \tag{2.5}$$

results in the nonlinear diffusion-type equation (2.1).

2.2. *Singularities*

The role of regularity conditions in relation to boundary conditions is discussed in §3.3. Hutter (1983, Chaps 5 and 6), emphasizes the issue and Fowler (1992) has constructed Frobenius expansions at the margin and the divide. We anticipate the tangent at the margin to be infinite and assume that the bed profile $b(x,t)$ is analytic at the margin. To leading order the flux at the margin is a constant, and thus from (2.4)

$$H \sim |x-S|^{v/(m+v)}, \quad x \leqslant S. \tag{2.6}$$

This expansion violates the reduced model assumptions as the derivatives are no longer $O(1)$, and we follow Fowler (1992), who argues that while the flow at the margin is incorrectly computed, the singular profiles which emerge from the use of the reduced model allow the flow in the rest of the ice sheet to be properly modelled.

The divide curvature is singular (Weertman 1961; Szidarovsky, Hutter & Yakowitz 1986; Fowler 1992) and we anticipate the need of an additional singular descriptor for divide asymmetry and motion. There are three requirements: (i) the slope is zero – under reduced model assumptions, this implies that the flux is zero; (ii) there is a non-zero vertical velocity, i.e. $\partial q/\partial x > 0$; (iii) there is an asymmetry which can lead to a non-zero divide migration rate. We are considering plane flow and thus we set $\omega \equiv 1$ for the rest of the section.

Setting the divide at the point $\partial_x s(x = x_d(t)) \equiv 0$, we may write

$$\left.\frac{\mathrm{D}(\partial_x s(x_d))}{\mathrm{D}t}\right|_{x=x_d} = \frac{\partial(\partial_x s)}{\partial t} + M_d\frac{\partial(\partial_x s)}{\partial x} = 0, \tag{2.7}$$

where M_d is the migration velocity of the divide. The differentiated form of the mass conservation condition is $\partial_x\partial_t s + \partial_x^2 q = \partial_x\partial_t b + \partial_x a$ and substituting this into (2.7) to eliminate $\partial_x\partial_t s$ yields

$$M_d\partial_x^2 s = \partial_x^2 q - \partial_x\partial_t b - \partial_x a. \tag{2.8}$$

Define a local coordinate $\hat{x} = x - x_d$, and set $\kappa = \mathrm{sgn}(x - x_d)$. We use a trial expansion about the moving divide

$$s = s_d \left(1 - e_1(\kappa\hat{x})^{1+1/v} + \kappa e_2(\kappa\hat{x})^{1+2/v}\right), \tag{2.9}$$

where the first two terms are the usual divide expansion (Fowler 1992) and the third term is the physically relevant descriptor of divide asymmetry and motion. The constants e_1 and e_2 emerge from solutions to (2.1), e_1 informing about the curvature of the divide and e_2 about the asymmetry of the divide. Assuming that b and a are analytic about the divide we can then compute

$$\begin{aligned}
\partial_x s &= -s_d \kappa e_1 (\kappa x)^{1/v} \left(1 - \frac{\kappa e_2 (v+2)}{e_1 (v+1)} (\kappa x)^{1/v}\right), \\
\partial_x^2 s &= -s_d \frac{(v+1)e_1}{v^2} (\kappa\hat{x})^{1/v-1} + \mathrm{O}(|\hat{x}|^{2/v-1}), \\
q &= Q \left(\hat{x} - \frac{v(v+2)e_2}{(v+1)e_1} (\kappa\hat{x})^{1+1/v}\right), \\
\partial_x q &= Q \left(1 - \kappa(v+2)\frac{e_2}{e_1} (\kappa\hat{x})^{1/v}\right), \\
\partial_x^2 q &= -Q \frac{e_2(v+2)}{e_1 v} (\kappa\hat{x})^{1/v-1},
\end{aligned}$$

where

$$Q \equiv s_d^{m+v} \left(\frac{e_1(v+1)}{v}\right)^v.$$

Substitution of the expressions for $\partial_x^2 s$ and $\partial_x^2 q$ into (2.8) shows that these are the leading-order terms as a result of the analyticity assumption for a and b, providing $v \neq 1$. Then, by calculating $M_d = \partial_x^2 q / \partial_x^2 H = \left(Q/s_d\right)\left(v(v+2)e_2/(v+1)e_1^2\right)$ we confirm that this is an $O(1)$ quantity. Clearly, stationary divides with flat bases have $e_2 = 0$.

2.3. *Linearization perturbation*

We construct a perturbation about a generalized VN solution, i.e. one with prescribed span S and with a non-zero flux out of the margin. We may then write

$$s(x,t) = s_0(x,t)\left(1 + \mu s_1(x,t)\right), \tag{2.10a}$$

$$\partial_x s(x,t) = \partial_x s_0(x)\left(1 + \mu\partial_x \left(s_0(x)s_1(x,t)\right)/\partial_x s_0(x)\right), \tag{2.10b}$$

$$H(x,t) = s_0(x)\left(1 + \mu s_1(x,t)\right), \tag{2.10c}$$

$$a = a_0(x) + \mu a_1(x). \tag{2.10d}$$

where μ is a small parameter. Since $s \sim s_0(1 + s_1)$, ensuring $s_1(x = S) = O(1)$ satisfies regularity conditions. Substitution of expansions (2.10) into (2.1) gives at zeroth order

$$\frac{1}{\omega}\partial_x \left(\omega C_0 s_0^m \left|\partial_x s_0\right|^{v-1} \partial_x s_0\right) + a_0 = 0, \tag{2.11}$$

when $\partial_t s_0 \equiv 0$. We can compute the first-order equation to be

$$\begin{aligned}
\frac{s_0}{(m+v)}\partial_t s_1 = &-\frac{1}{\omega}\partial_x \left(\omega q_0 \left\{s_1 + \frac{v}{m+v}\frac{s_0}{\partial_x s_0}\partial_x s_1\right\}\right) \\
&+ \frac{1}{m+v} a_1 + O\left(\mu\frac{mv}{m+v}\right).
\end{aligned} \tag{2.12}$$

Note that the zeroth-order rate factor does not enter explicitly into this equation; this is useful, as very often the flux is the measurable quantity. This form is also the more convenient for error analysis, showing that the error for s_1 is $O\left(\mu mv/(m+v)\right)$. Typically, $mv/(m+v) \approx 2$, meaning that if the acceptable error in s_1 is 10%, then $\mu = 0.05$, i.e. we can consider deviations from the base profile of 5% for this error. It is apparent from the above equation that this will be the result of forcings a_1 of magnitude $\mu(m+v)$, which for $v = 3, \mu = 5$ is a forcing perturbation of 40%. This means that we can expect to be able to use linearizations to compute ice-sheet evolutions of practical interest. Equation (2.12) can be written in a form convenient for Sturm–Liouville analysis of associated eigenvalue problems:

$$\frac{s_0}{(m+v)}\partial_t s_1 + \frac{1}{s_0^{(m+v)/v}\omega}\partial_x\left(\omega q_0 \frac{v}{m+v}\frac{s_0^{1+(m+v)/v}}{\partial_x s_0}\partial_x s_1\right) = -\frac{\partial_x(\omega q_0)}{\omega}s_1 + \frac{a_1}{m+v} + O\left(\mu\frac{mv}{m+v}\right). \tag{2.13}$$

Both forms of the linearized equation are useful: (2.12) demonstrates qualitative properties (e.g. the error analysis, the robustness to model perturbation, see §4.4), while (2.13) is of direct use in the following analysis.

3. Sturm–Liouville analysis of perturbations about the Vialov–Nye solution

3.1. *VN solution as the zeroth-order equation*

The zeroth-order equation (2.11) integrates to

$$q_0(x) = -\omega C_0 s_0^m \left|\partial_x s_0\right|^{v-1}\partial_x s_0 = \int_0^x a_0 \omega \mathrm{d}x'. \tag{3.1}$$

We treat a_0, C_0, as being constant and ω having power-law dependence on x, i.e. $a_0(x) = a_m, C_0(x) = C_m, x$,and $\omega(x) = |x/S|^d$. The cases $d = 0, 1$ correspond to plane flow and axisymmetric flows. It is not realistic to have the zeroth-order fields as constants – the rate factor C can vary by several orders of magnitude, which cannot be modelled as a perturbation. However, a perturbation can indicate the sensitivity of a solution to parameter variation.

Integration of (3.1) using a monotonicity condition $\mathrm{sign}(\partial_x s_0) = -1$ with the boundary condition $s_0(S) \equiv 0$ yields the VN solution

$$s_d = \left(S^\delta\left(\frac{\gamma+1}{\delta}\right)^v\left(\frac{a_m}{C_m(d+1)}\right)\right)^{1/(\gamma+1)}, \tag{3.2a}$$

$$s_0(x) = s_d\left(1 - |x/S|^{\delta/v}\right)^{v/(\gamma+1)}. \tag{3.2b}$$

where $\gamma \equiv m + v - 1, \delta \equiv v + 1$. This profile (3.2) is plotted in figure 1 for a few cases, demonstrating the small sensitivity of ice-sheet profile to parameter variation. It is a straightforward exercise to show that the profile satisfies the margin regularity condition (2.6) and the first two (i.e. even) terms of the divide regularity condition (2.9), with $e_1 = \delta/(\gamma+1), e_2 = 0$.

3.2. *Rescaling for Sturm–Liouville form*

It is very desirable in the ensuing Sturm–Liouville analysis to have the field equation solved on a domain $[0, 1]$, and it also makes life a lot easier if we ensure that

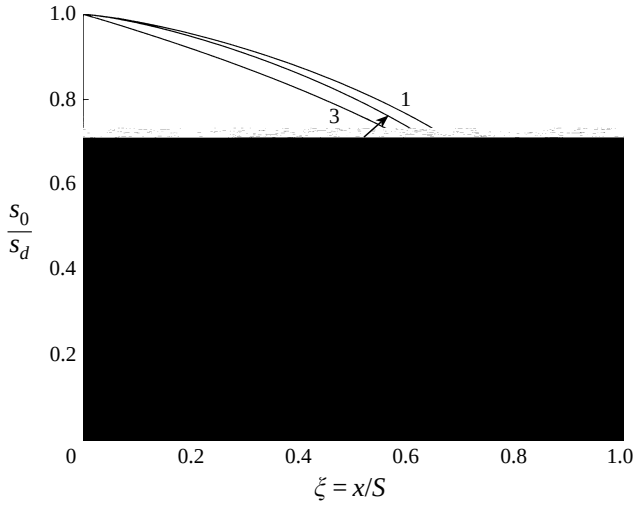

FIGURE 1. Normalized zeroth-order profile s_0/s_d for the VN solution. Cases (1) $v = 3, \delta = 4, \gamma = 7$ (i.e. spreading by Glen internal deformation); (2) $v = 3, \delta = 4, \gamma = 6$ (spreading by Weertman sliding); (3) $v = 3, \delta = 3, \gamma = 7$ (spreading by Glen internal deformation with rate factor increasing from centre).

zeroth-order ice-sheet profile is also normalized; thus we define

$$\xi \equiv x/S, \tag{3.3a}$$

$$\eta_0(\xi) \equiv s_0(x)/s_d, \tag{3.3b}$$

$$\eta_1(\xi, t) \equiv s_1(x, t), \tag{3.3c}$$

and the VN profile (3.2) becomes

$$\eta_0(\xi) = \left(1 - |\xi|^{\delta/v}\right)^{v/(\gamma+1)}. \tag{3.4}$$

Using this substitution (3.3), the ice-sheet evolution equation (2.1) becomes

$$s_d \partial_t \eta = \frac{1}{\omega} \frac{s_d^{m+v}}{S^\delta} \partial_\xi \left(\omega C \eta^m |\partial_\xi \eta|^{v-1} \partial_\xi \eta\right) + a,$$

with the flux

$$q = -\frac{s_d^{m+v}}{S^v} \omega C \eta^m |\partial_\xi \eta|^{v-1} \partial_\xi \eta.$$

After using the identity $m + v = \gamma + 1$, the perturbation equation (2.13) then becomes

$$\frac{s_d \eta_0}{a_0(\gamma+1)} \partial_t \eta_1 + \frac{1}{\xi^d \eta_0^{(\gamma+1)/v}} \partial_\xi \left(\xi^{d+1} \frac{v}{\gamma+1} \frac{\eta_0^{1+(\gamma+1)/v}}{\partial_\xi \eta_0} \partial_\xi \eta_1\right) = -(d+1)\eta_1 + \frac{a_1}{(\gamma+1)a_0} + O\left(\mu \frac{mv}{\gamma+1}\right). \tag{3.5}$$

3.3. *Sturm–Liouville theory: some definitions*

Having constructed linearized equations by using the VN profile as the zeroth-order solution, they are most conveniently analysed in Sturm–Liouville form (Birkhoff & Rota 1989). Consider a second-order eigenvalue problem

$$\partial_x(\mathscr{T}(x)\partial_x U) - \mathscr{Q}(x) U - \mathscr{W}(x) \lambda U = 0 \tag{3.6}$$

where $\mathscr{T}(x)$ is the transmission function, $\mathscr{Q}(x)$ is a potential function and $\mathscr{W}(x)$ is the weighting or storage function. Boundary conditions are prescriptions of U or of the generalized flux $-\mathscr{T}(x)\,\partial_x U$. When the functions $\mathscr{T}, \mathscr{Q}, \mathscr{W}$ are singular at the boundaries, U is not analytic and is expanded in a Frobenius series in order to satisfy the boundary conditions. The leading-order terms are chosen so as to satisfy regularity conditions on certain quantities, in this case the flux, which is a conserved quantity. Equation (3.6) has eigenfunction solutions $\mathscr{E}_i(x), i \in \mathbb{N}$ which are orthonormal with respect to the weighting function, i.e. $\int \mathscr{E}_i(x)\,\mathscr{W}(x)\,\mathscr{E}_j(x)\,\mathrm{d}x = \delta_{ij}$ where δ_{ij} is the Kronecker delta.

Consider now the related partial differential equation

$$\mathscr{W}(x)\,\partial_t V = \partial_x\left(\mathscr{T}(x)\,\partial_x V\right) - \mathscr{Q}(x)\,V + \mathscr{S}(x)\,\mathscr{F}(x). \tag{3.7}$$

Here, $\mathscr{F}(x)$ will be a forcing function with some physical meaning – for example the first-order accumulation a_1, while the function $\mathscr{S}(x)$ emerges from the analysis. A standard separation of variable technique setting $V(x,t) = U(x)T(t)$ transforms the homogeneous form of (3.7), where the forcing is zero, into two ordinary differential equations, the spatial one being in Sturm–Liouville form like (3.6). The eigenfunction solutions form a complete set so we may write solutions in the form $V = \sum_{i=1}^{\infty} T_i \mathscr{E}_i$ and using a standard derivation (e.g. Hindmarsh 1996) construct mode-evolution equations

$$\dot{T}_j = \lambda_j T_j + \int \mathscr{E}_j \mathscr{S} \mathscr{F}\,\mathrm{d}y, \;\; j \in \mathbb{N} \tag{3.8}$$

where λ_j is the corresponding eigenvalue. By defining a Green's function

$$\mathsf{G}(x,y) = \mathsf{G}(y,x) = \sum_{k=1}^{\infty} \frac{\mathscr{E}_i(x)\,\mathscr{E}_j(y)}{-\lambda_j} \tag{3.9}$$

we may solve the non-homogeneous steady equation through $V(x,\infty) = \int \mathsf{G}(x,y)\,\mathscr{S}(y)\,\mathscr{F}(y)\,\mathrm{d}y$. One may also write the quadrature formula as

$$V(x,\infty) = \int \mathsf{K}(x,y)\,\mathscr{F}(y)\,\mathrm{d}y, \quad \mathsf{K}(x,y) = \mathsf{G}(x,y)\,\mathscr{S}(y) \tag{3.10}$$

in terms of a non-symmetric kernel K we call the influence function.

3.4. *Symmetric perturbation*

Substituting (3.4) into (3.5), multiplying the result by $\delta \xi^d \eta_0^{(\gamma+1)/v}/v$ and defining some new constants

$$R_s = \frac{a_m \Lambda_s}{s_d}, \;\; \Lambda_s = \frac{v(\gamma+1)}{\delta} \tag{3.11}$$

allows us to rewrite the evolution equation (3.5) as

$$\frac{1}{R_s}\mathscr{W}\partial_t \eta_1 = \partial_\xi\left(\mathscr{T}\partial_\xi \eta_1\right) - \mathscr{Q}\eta_1 \; + \frac{\mathscr{S}(\xi)\,\mathscr{F}_1}{\Lambda_s a_m} + O\left(\frac{\delta m}{\gamma+1}\mu\right), \tag{3.12a}$$

$$\mathscr{W} = \xi^d\left(1-\xi^{\delta/v}\right)^{1+v/(\gamma+1)}, \quad \mathscr{Q} = (d+1)\,\delta\xi^d\left(1-\xi^{\delta/v}\right)/v, \tag{3.12b,c}$$

$$\mathscr{T} = \xi^{d+2-\delta/v}\left(1-\xi^{\delta/v}\right)^2, \quad \mathscr{S} = \xi^d\left(1-\xi^{\delta/v}\right), \quad \mathscr{F}_1 = a_1. \tag{3.12d–f}$$

Then, construction of the separable form $\eta_1(\xi,t)=\Theta(\xi)T(t)$ allows us, after setting F to zero, to rewrite the homogenous equation corresponding to (3.12a) as

$$\frac{1}{R_s}\frac{T'}{T}=\lambda^s=\frac{1}{\mathscr{W}}\left(\partial_\xi\left(\mathscr{T}\partial_\xi\Theta\right)-\mathscr{Q}\Theta\right), \tag{3.13}$$

yielding ordinary differential equations

$$T'(t)=\lambda^s R_s T(t) \tag{3.14}$$

and

$$\partial_\xi\left(\mathscr{T}\partial_\xi\Theta\right)-\left(\mathscr{Q}+\lambda^s\mathscr{W}\right)\Theta=0. \tag{3.15}$$

The boundary conditions corresponding to zero flux (divide) and zero thickness (margin) enter as regularity conditions. The end-point singularities in this equation are not Fuchsian and numerical solution is required. Substitution of a trial expansion $\Theta=\xi^c$ in equation (3.15) yields indicial equations with solutions $c=0, c=\delta/v-d-1$. The first solution satisfies the boundary conditions of zero flux. The indicial equation for the expansion about the margin has solutions $c=-1,0$. The solution $c=0$ satisfies the boundary conditions and this solution is also adopted by the Green's function.

3.5. *Antisymmetric perturbation*

The singularity in divide curvature prevents a regular antisymmetric perturbation, and a stretched coordinate system is used to deal with this problem following Halfar (1981). He found infinite tangents at the divide, but by respecting the regularity condition for an antisymmetric divide (2.9) we avoid this behaviour. We define the stretching coordinate ξ such that

$$\eta(\xi,t)=\eta_0(\xi_*),\ \xi=X(\xi_*,t_*), \tag{3.16}$$

and solve for ξ, the physical coordinate, with ξ_*, t as the independent variables. The divide position is given by $\xi(0,t)$. In terms of the starred coordinate system the transforms are

$$\frac{\partial\eta}{\partial t}\frac{\partial t}{\partial t_*}+\frac{\partial\eta}{\partial\xi}\frac{\partial X}{\partial t_*}=\frac{\partial\eta_0}{\partial t_*}=0,\quad \frac{\partial\eta}{\partial\xi}\frac{\partial X}{\partial\xi_*}=\frac{\partial\eta_0}{\partial\xi_*},\quad \frac{\partial}{\partial\xi}\frac{\partial X}{\partial\xi_*}=\frac{\partial}{\partial\xi_*}.$$

and we use the transform for $\partial\eta/\partial\xi$ to construct that for $\partial\eta/\partial t$,

$$\frac{\partial\eta}{\partial t}=-\left(\frac{\partial\eta_0}{\partial\xi_*}\Big/\frac{\partial X}{\partial\xi_*}\right)\frac{\partial X}{\partial t_*},$$

where we have also used $\partial t_*/\partial t\equiv 1$. Instead of an evolution equation for η_1, see (2.1) we obtain an evolution equation for $X(\xi_*,t)$,

$$-s_d\left(\frac{\partial\eta_0}{\partial\xi_*}\Big/\frac{\partial X}{\partial\xi_*}\right)\frac{\partial X}{\partial t_*}=\frac{1}{S}\frac{\partial}{\partial\xi_*}\left(q_0(\xi_*)\left|\frac{\partial X}{\partial\xi_*}\right|^{-(v+1)}\frac{\partial X}{\partial\xi_*}\right)\Big/\frac{\partial X}{\partial\xi_*}+a. \tag{3.17}$$

We linearize, perturbing the stretched coordinate system with small parameter μ,

$$\xi=X(\xi_*,t_*)\simeq\xi_*+\mu X_1(\xi_*,t_*), \tag{3.18}$$

and find

$$\frac{\partial X}{\partial t_*}\simeq\mu\frac{\partial X_1}{\partial t_*},\quad \frac{\partial X}{\partial\xi_*}=1+\mu\frac{\partial X_1}{\partial\xi_*}. \tag{3.19}$$

We fix the margin position by setting $X_1(1,t)=0$, while the value of $X_1(0,t)$ determines the position of the divide in ξ-space.

We construct antisymmetric perturbations in the accumulation rate

$$a \simeq a_0 + \mu a_1(\xi_*, t_*). \tag{3.20}$$

Substituting (3.18), (3.19) into the evolution equation (3.17) gives us the zeroth-order identity $-\partial(a_0\xi_*)/\partial\xi_* + a_0 = 0$. Taking $(v-1)/2 = O(1)$, the evolution equation for X_1 is

$$\frac{1}{R_a}\mathscr{W}\partial_t X_1 = \partial_{\xi_*}\left(\mathscr{T}\partial_{\xi_*}X_1\right) + \frac{\mathscr{S}\mathscr{F}_1}{a_m} + O(\mu), \quad \xi_* \in [0,1], \tag{3.21a}$$

$$\mathscr{W} = \left(1-\xi_*^{\delta/v}\right)^{v/(\gamma+1)-1}\xi_*^{2/v}, \tag{3.21b}$$

$$\mathscr{T} = \xi_*^{1+1/v}, \tag{3.21c}$$

$$\mathscr{S} = \xi_*^{1/v}/v, \tag{3.21d}$$

$$\mathscr{F}_1 = a_1, \tag{3.21e}$$

$$R_a = \frac{a_m v(\gamma+1)}{s_d\delta}, \tag{3.21f}$$

where X_1 is an even function about zero, satisfying regularity conditions at the divide and being set to zero at the margin.

We treat the homogeneous problem with $X_1(\xi_*, t_*)$ in separated form:

$$X_1(\xi_*, t_*) = X_*(\xi_*)T_*(t_*), \tag{3.22}$$

and substitute this into (3.21) to obtain

$$\frac{1}{\Lambda_a}\frac{\dot{T}_*}{T_*} = \lambda^a = \frac{\partial_{\xi_*}\left(\mathscr{T}\partial_{\xi_*}X_*\right)}{\mathscr{W}X_*},$$

where λ^a is the eigenvalue of the problem. The time equation has solution $T_* = T_{*0}\exp(\lambda^a\Lambda_1 t_*)$, where T_{*0} represents an initial condition, and the second-order equation in space can be written as

$$\frac{\partial}{\partial\xi^*}\left(\mathscr{T}\frac{\partial X_*}{\partial\xi_*}\right) - \lambda^a\mathscr{W}X_* = 0. \tag{3.23}$$

At the divide the indicial equation corresponding to the trial expansion $X_* = \xi_*^c$ yields

$$c = 0, -1/v \tag{3.24}$$

with $c=0$ satisfying the boundary conditions for the stretching problem, while at the margin the solution to the indicial equation is $c = 0, 1$ with $c = 1$ satisfying the boundary conditions. An important point which will emerge is that the Green's function, which must also satisfy the indicial equation, is singular at the divide.

3.6. *Numerical solutions to the eigenproblem*

Numerical methods for solving Sturm–Liouville problems are discussed by Pryce (1993). We compare two methods: (i) Pruess-type methods based upon the Prüfer sub-

stitution and (ii) finite difference discretizations into a matrix equation and the solution of the corresponding algebraic eigenvalue problem. Shooting methods are usually superior, especially for high wavenumbers, but in future work we will be considering higher dimensional perturbations, where finite-difference discretizations are more convenient. For shooting we used a public-domain code SLEDGE (Pruess & Fulton 1993), which contains an automatic end-point analyser for singularities and non-analyticity.

In the finite difference discretization to the symmetric problem we consider the eigenvalue problem (3.15) in a transformed coordinate $\theta = \xi^{\delta/\nu}$ (the Halfar transform) which removes the divide singularity, and we expand in the form $\Theta = c_0 + c_1\theta$. Substitution of this into the transformed second-order ODE corresponding to (3.15) and solving for c_0, c_1 yields $((d+1)\nu/\delta\Delta_\theta)(\Theta_1 - \Theta_0(1+\Delta_\theta)) - \lambda^s\Theta_0 = O\left(\Delta_\theta^2\right)$. At the margin where we use the expansion $\hat{\Theta} = c_0 + c_1\hat{\theta} + c_2\hat{\theta}^{\nu/(\gamma+1)+1}$, $\hat{\theta} \equiv 1 - \theta$, where c_0 etc. are different from the quantities used in the divide case. Here, Δ represents the discretization interval, with the subscript indicating the independent variable. Expanding the transformed equation around $\hat{\theta} = 0$ and solving for c_i yields the $(N+1)$th row of the matrix equation

$$\Theta_{N-1} = \Theta_N\left(\frac{\lambda^s\Delta_\theta^{\nu/(\gamma+1)+1}}{\Gamma} + 1 + \frac{\nu(d+1)}{2\delta}\Delta_\theta\right),$$

$$\Gamma = \frac{(\nu+\gamma+1)}{\gamma+1}\left(2 + \frac{\nu}{(\gamma+1)}\right).$$

At the $N-1$ interior points, the second-order ODE is written in the form

$$\frac{1}{\mathscr{W}(\theta)}\frac{\mathrm{d}}{\mathrm{d}\theta}\left(\mathscr{T}(\theta)\frac{\mathrm{d}\Theta}{\mathrm{d}\theta}\right) - \left(\frac{\nu(d+1)}{\delta\eta_0} + \lambda^s\right)\Theta = 0$$

where $\mathscr{T}(\theta) \equiv \theta^{\nu(d+1)/\delta}(1-\theta)^2$, $\mathscr{W}(\theta) = \theta^{\nu d-1/\delta}(1-\theta)^{1+\nu/(\gamma+1)}$. A discretized flux-conservative form is used, with $\mathscr{T}(\theta)$ evaluated at grid centres $\left(i \pm \frac{1}{2}\right)\Delta_\theta$ and $\mathscr{W}(\theta)$ evaluated at grid points $i\Delta_\theta$.

In the discretization of the antisymmetric equation at the margin the boundary condition is $X_1 = 0$. At the divide we satisfy the expansion (2.9) by $X_* = X_{*0} + c_1\xi_*^{1+1/\nu}$, where X_{*0} represents the value of X_* at the divide. This yields a discretized relationship

$$\frac{(1+1/\nu)(1+2/\nu)}{\Delta_\xi^{1+1/\nu}}(X_{*1} - X_{*0}) - \lambda^a X_{*0} = 0.$$

At the rows comprising the interior points the discretization is the obvious one for a linear self-adjoint equation.

The usual effect of discretization error is to create inaccuracies in the spectrum at high wavenumber, with a concomitant effect on the corresponding eigenfunctions (Pryce 1993). Finite difference discretizations of regular Sturm–Liouville equations yield error estimates of $O\left(k^4\Delta_\xi^2\right)$, and this estimate is likely to be optimistic for irregular equations. Courant & Hilbert (1953, Vol. 1, p. 415), show that

$$\lim_{k\to\infty}\frac{k^2}{\lambda_k} = \frac{1}{\pi^2}\left(\int_0^1\left(\frac{\mathscr{W}(\xi_*)}{\mathscr{T}(\xi_*)}\right)^{1/2}\mathrm{d}\xi_*\right)^2,$$

where we recall (Birkhoff & Rota 1989, pp. 417–419) that the zeros of the kth

v	δ	γ	d	Geom	FD1	PP1	FD2	PP2	FD3	PP3	$\frac{An\infty}{k^2}$	$\frac{PP\infty}{k^2}$	Type
3	4	7	0	S	9.11	9.11	49.8	49.7	123	123	16.4	16.3	D
3	4	7	0	A	16.2	16.2	64.9	65.0	146	146	16.4	16.4	D
3	4	7	1	X	20.0	20.0	72.8	72.8	158	158	16.4	16.4	D
3	4	6	0	S	8.11	8.10	45.1	45.0	112	112	15.1	15.0	S
3	4	6	0	A	14.5	14.5	58.9	59.0	133	134	15.1	15.1	S
3	4	6	1	X	18.0	18.0	66.1	66.2	144	144	15.1	15.1	S
1	2	3	0	S	4.27	4.27	29.2	29.2	75.8	75.7	10.8	10.8	D
1	2	3	0	A	14.0	14.0	49.7	49.7	107	107	10.8	10.9	D
1	2	3	1	X	8.97	8.97	39.3	39.3	91.2	91.3	10.8	10.8	D
4	5	9	0	S	11.6	11.6	61.0	61.0	150	150	19.6	19.6	D
4	5	9	0	A	18.3	18.3	75.6	75.6	172	172	19.6	19.6	D
4	5	9	1	X	25.6	25.6	90.7	90.7	195	195	19.6	19.7	D

TABLE 1. Comparison of finite difference (FD) and Prüfer–Pruess (PP) methods for finite eigenvalue calculation, and PP and analytical solutions for asymptotic eigenvalues. The number after FD, PP corresponds to the eigenvalue ordinal k. Geometries are symmetric (S), antisymmetric (A) and axisymmetric (X). Finite difference calculations used 100 grids, PP calculations a tolerance of 10^{-3}. Types of flow are internal deformation (D) and sliding (S). See text for explanation of the parameters v, δ, γ and d. Columns 12 and 13 represent λ/k^2 as $\lim k \to \infty$ for the analytical asymptotic solution and as calculated by PP methods. PP calculations had a tolerance of 10^{-3}, and show λ/k^2 for $k = 100$.

eigenfunction divides the interior of the domain into k regions. We find

$$\lim_{k\to\infty} \frac{k^2}{\lambda_k^s} = \lim_{k\to\infty} \frac{k^2}{\lambda_k^a} = \frac{1}{\pi^2}\left(\frac{v}{\delta} B\left(\frac{1}{2}, \frac{1}{2} + \frac{v}{2(\gamma+1)}\right)\right)^2 \tag{3.25}$$

where B is the beta function. (The equivalence of these results is a necessary condition for having computed the perturbations correctly.) We validate by comparing computed asymptotic spectra with this result.

Our major concerns are: (i) computing the first few eigenvalues and eigenfunctions, as these give the response times of the most important modes; (ii) carrying out sufficient testing to demonstrate that these have been computed correctly; (iii) computing the influence functions, which requires a long eigenfunction expansion.

We see from table 1 that near three-figure accuracy is being obtained, and that the eigenvalues for the slowest mode tend to lie somewhat higher than the value of $\gamma + 1$ predicted from scale theory. The slowest antisymmetric modes have eigenvalues approximately twice the fundamental eigenvalue. The comparisons of computed and analytic asymptotic spectra show excellent agreement.

3.7. *Perturbations of bed profile and rate factor*

In addition to perturbing the accumulation rate, linearization can also be used to perturb the rate factor C and the bed profile $b(x, t)$. We write

$$\begin{aligned} C &= C_0(x) + \mu C_1(x), \\ b &= b_0(x) + \mu b_1(x), \\ H(x,t) &= s_0(x)\,(1 + \mu s_1(x,t)) - \mu b_1(x), \end{aligned}$$

and it is easy to compute that the forcing for the general VN perturbation (2.13) is now given by

$$\frac{s_0}{\gamma+1}\partial_t s_1 + \frac{1}{\omega s_0^{(\gamma+1)/\nu}}\partial_x\left(\omega q_0 \frac{\nu}{\gamma+1}\frac{s_0^{1+(\gamma+1)/\nu}}{\partial_x s_0}\partial_x s_1\right) = -\frac{\partial_x(\omega q_0)}{\omega}s_1 + \frac{F_1}{\gamma+1} + O\left(\mu\frac{m\nu}{\gamma+1}\right), \tag{3.26a}$$

$$F_1 = a_1 - \frac{1}{\omega}\partial_\xi\left(\omega q_0\left(\frac{C_1}{C_0} - m\frac{b_1}{s_0}\right)\right). \tag{3.26b}$$

Similar computations reveal the forcing functions for the symmetric and antisymmetric perturbations to the VN solution (equations (3.12*a*), (3.21*a*)) to be

$$\mathscr{F}_1(\xi,t) = a_1(\xi) - \frac{a_m}{\xi^d}\partial_\xi\left(\xi^{d+1}\left\{\frac{C_1}{C_0} - m\frac{b_1}{s_0}\right\}\right). \tag{3.27}$$

3.8. *Green's and influence functions for steady perturbations*

With $\mathscr{S}(\xi) = \xi^d(1-\xi^{\delta/\nu})$ for the symmetric case we have from (3.10) an influence function defined as

$$K(\xi,\phi) = \sum_{i=1}^{\infty}\frac{\mathscr{E}_i(\xi)\,\mathscr{E}_i(\phi)\,\phi^d\left(1-\phi^{\delta/\nu}\right)}{-\lambda_i},$$

which we can use to write the true perturbation

$$\hat{\eta}_1 = \eta_0\eta_1 = \frac{1}{\Lambda_{s1}}\int_0^1 \eta_0\sum_{i=1}^{\infty}\frac{\mathscr{E}_i(\xi)\,\mathscr{E}_i(\phi)}{-\lambda_i}\phi^d\left(1-\phi^{\delta/\nu}\right)a_1(\phi)\,\mathrm{d}\phi,$$

with corresponding influence function

$$K_a^s(\xi,\phi) = \eta_0\sum_{i=1}^{\infty}\frac{\mathscr{E}_i(\xi)\,\mathscr{E}_i(\phi)}{-\lambda_i\Lambda_{s1}}\phi^d\left(1-\phi^{\delta/\nu}\right). \tag{3.28}$$

The rate-factor perturbation $(a_{m0}/\xi^d)\partial_\xi\left\{\xi^{d+1}C_1(\xi)\right\}$ (see (3.27)) appears inside a derivative, and to compute an influence function we integrate the product of this term and K_a^s by parts, obtaining

$$K_C^s(\xi,\phi) = -\eta_0(\xi)\sum_{i=1}^{\infty}\left(\frac{\mathscr{E}_i(\xi)\,\mathscr{E}_i(\phi)}{-\lambda_i\Lambda_s}\right)\frac{\delta}{\nu}\phi^{d+\delta/\nu} + \eta_0(\xi)\sum_{i=1}^{\infty}\left(\frac{\mathscr{E}_i(\xi)\,\mathscr{T}(\phi)\,\partial_\phi\mathscr{E}_i(\phi)}{-\lambda_i\Lambda_s}\right)\frac{\phi^{1/\nu}}{1-\phi^{\delta/\nu}}. \tag{3.29}$$

With $\mathscr{S}(\xi_*) = \xi_*^{1/\nu}/\nu$ for the antisymmetric case we have from (3.10) the influence function for the accumulation perturbation

$$K_a^a(\xi_*,\phi) = \frac{1}{\nu a_0}\sum_{i=1}^{\infty}\frac{\mathscr{E}_i(\xi_*)\,\mathscr{E}_i(\phi)}{-\lambda_i}\phi^{1/\nu}, \tag{3.30}$$

which yields $X_1(\xi_*)$. The perturbation to the profile is recovered by using the leading-order relationship $\hat{\eta}_1 \simeq -(\partial\eta_0/\partial\xi_*)X_1(\xi_*)$. The rate factor perturbation influence

function is

$$K_C^a(\xi_*, \phi) = \frac{1}{\nu} K_a^a + \frac{1}{\nu} \sum_{k=1}^{\infty} \frac{\mathscr{E}_i(\xi)\, \mathscr{T}(\xi)\, \partial_\phi \mathscr{E}_i(\phi)}{-\lambda_j}. \tag{3.31}$$

4. Applications

4.1. *Computation of the influence function*

The influence functions were computed using summations of eigenfunction series generated by SLEDGE. In all cases 200 eigenfunctions were used, each represented by 807 points (symmetric case) and 808 points (antisymmetric case). These are sufficient to represent the break in slope found by definition in Green's and related influence functions (Roach 1982) but there are still Gibbs' phenomena associated with the computation of K_C^a. These do not appear to jeopardise the accuracy of the response obtained by convolving the influence functions with the forcing, as indicated by cross-checks on the computation of the influence functions, which may be made as follows. Following Weertman (1973), Hindmarsh (1996) shows the ratio of distances from divide to left and right margins S_L, S_R are given by

$$\frac{S_L}{S_R} = \Upsilon = \left(\frac{(a_{mR}/a_{mL})}{(C_{mR}/C_{mL})} \right)^{1/\delta},$$

where subscripts L,R represent values on left and right sides. We may easily show from this relation and (3.2) that

$$\frac{\mathrm{d}s_d}{\mathrm{d}a_m} = \frac{1}{\gamma+1} \frac{s_d}{a_m}, \quad \frac{\mathrm{d}X_0}{\mathrm{d}a_{mR}} = \frac{1}{\delta(1+\Upsilon)^2} \frac{\Upsilon}{a_{mR}}, \tag{4.1}$$

where X_0 is the normalized divide-position deviation. By setting the accumulation perturbation a_1 to be a constant and using (3.28), (3.30) we should recover the relationships (4.1). Thus, for the symmetric case, setting $a_1(\phi) = a_{1c}$ we expect to find

$$\hat{\eta}_1 = \frac{1}{\Lambda_{s1}} \int_0^1 \eta_0 \sum_{i=1}^{\infty} \frac{\mathscr{E}_i(\xi)\, \mathscr{E}_i(\phi)}{-\lambda_i} \phi^d \left(1 - \phi^{\delta/\nu}\right) a_{1c} \mathrm{d}\phi = \frac{a_{1c}}{\gamma+1} \eta_0,$$

and for the antisymmetric case we expect

$$X_1(\xi_*) = \frac{1}{\nu a_0} \int_0^1 \sum_{i=1}^{\infty} \frac{\mathscr{E}_i(\xi_*)\, \mathscr{E}_i(\phi)}{-\lambda_i} \phi^{1/\nu} a_{1c} \mathrm{d}\phi = \frac{a_{1c}}{\delta} (1 - \xi_*).$$

The solutions (4.1) were obtained with errors of $< 10^{-5}$. The solutions for unit perturbations in rate factor are

$$\hat{\eta}_1 = -\frac{C_{1c}}{\gamma+1} \eta_0, \quad X_1 = -\frac{C_{1c}}{\delta} (1 - \xi_*)$$

respectively. The errors for all these were very small ($\lesssim 10^{-4}$), even for the rate-factor perturbation to the antisymmetric solution, which suffers from Gibbs' phenomena. We comment that the step function in accumulation rate at the divide for the antisymmetric case violates the assumption of analyticity, but this does not have significantly deleterious consequences.

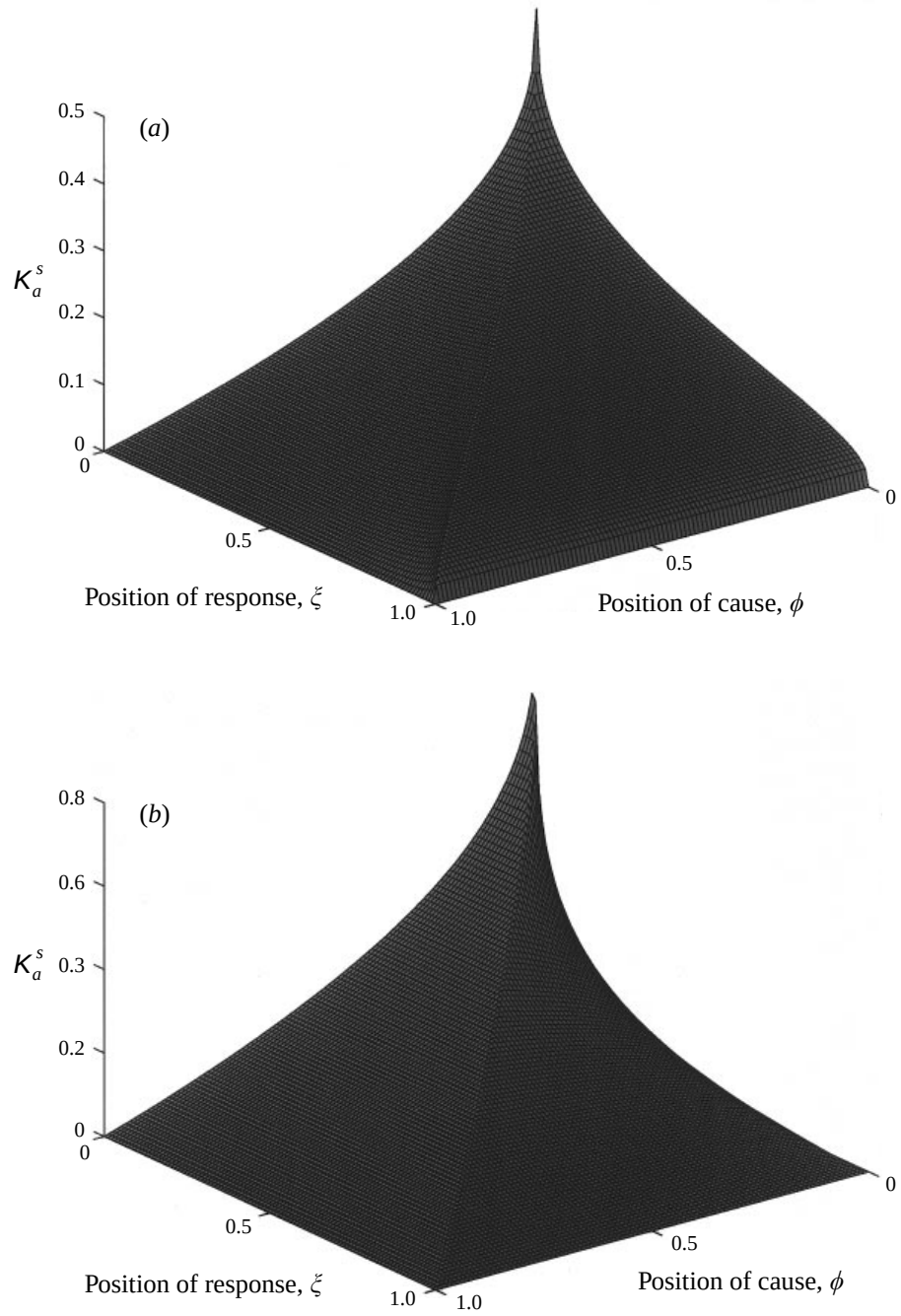

FIGURE 2. Accumulation rate influence function (*a*) $K_a^s(\xi, \phi)$ for the symmetric base case (*b*) $K_a^a(\xi, \phi)$ for the anti-symmetric base case $\nu = 3$, $\delta = 4$, $\gamma = 7$, $d = 0$.

4.2. *Sensitivity to spatial variation in forcing fields*

The physical interpretation of the influence function for the symmetric (figure 2*a*) and anti-symmetric (figure 2*b*) perturbations is a delta-function impulse being applied to the system at a position ϕ on the influence axis which produces the indicated response along the ξ-axis, samples of which are plotted in figure 3. The influence

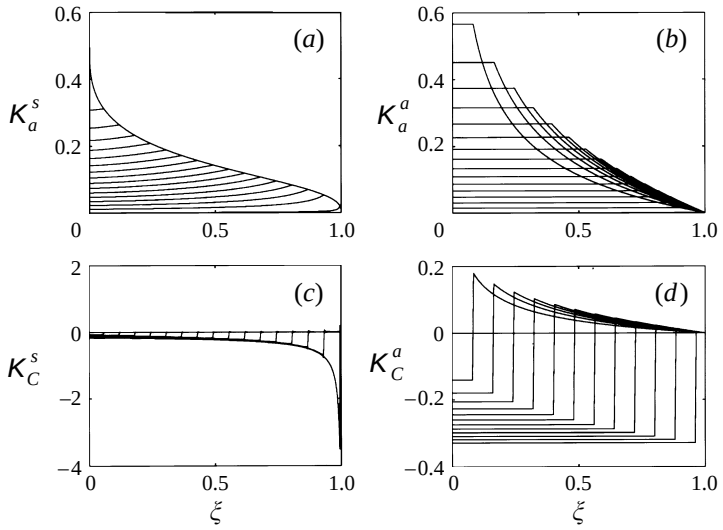

FIGURE 3. Samples of the kernel influence functions for constant ϕ. Horizontal axis is ξ, the response axis. The value of ϕ is indicated by the position of the break in slope of the function. (*a*) Symmetric accumulation perturbation $K_a^s(\xi, \phi)$, (*b*) Antisymmetric accumulation perturbation $K_a^a(\xi, \phi)$, (*c*) Symmetric rate-factor perturbation $K_C^s(\xi, \phi)$, (*d*) Anti-symmetric rate factor perturbation $K_C^a(\xi, \phi)$. All for the case $v = 3$, $\delta = 4$, $\gamma = 7$ and $d = 0$.

functions, which indicate spatial sensitivity, exhibit typical forms for diffusion-type equations, with maximum sensitivity found at the centre $\xi = 0$ and a declining sensitivity of profile along the diagonal $\xi = \phi$ found as one moves to the margin. The divide-position sensitivity kernel function $K_a^a(0, \phi)$ to antisymmetric accumulation distributions is shown in figure 4. The principal qualitative feature is that of greater sensitivity near the divide. The indicial equation solution (3.24) indicates the possibility of singular behaviour in the Greens function K_a^a, which does not converge uniformly at the divide. The analytical check based on (4.1) indicates that failure to model this singularity properly is not of numerical significance.

The sensitivity of the volume perturbation $\int_0^1 \eta_1 \mathrm{d}\phi$ to symmetric accumulation perturbation is expressed through the kernel influence function V_a:

$$V_a(\phi) = \int_0^1 K_a^s(\xi, \phi)\mathrm{d}\xi, \quad \int_0^1 \eta_1 \mathrm{d}\phi = \int_0^1 V_a(\phi) a_1 \mathrm{d}\phi.$$

This is plotted in figure 4. There is a decreasing sensitivity on volume perturbation with distance from divide as predicted from recursion relationships by Hindmarsh (1992). The volume sensitivity function can be regarded as an ideal sampling density function. Accumulation rate measurements designed to constrain glaciological response should have a higher density in the central area of an ice sheet.

The forms of the influence functions for rate factor and basal topography normalized by the local ice-sheet thickness are the same (figure 5), although the influence function should be multiplied by $-m$ in assessing the response to a forcing $-b_1/s_0$. These influence functions for very long-wavelength topography complement those computed by Jóhannesson (1992) for medium and short wavelengths. The Neuman summation used in the computation of K_C^a produced severe Gibbs' phenomena, and for the purpose of illustration we use the less accurate method of inverting the finite difference operator whose construction was outlined in §3.6. In computation, the

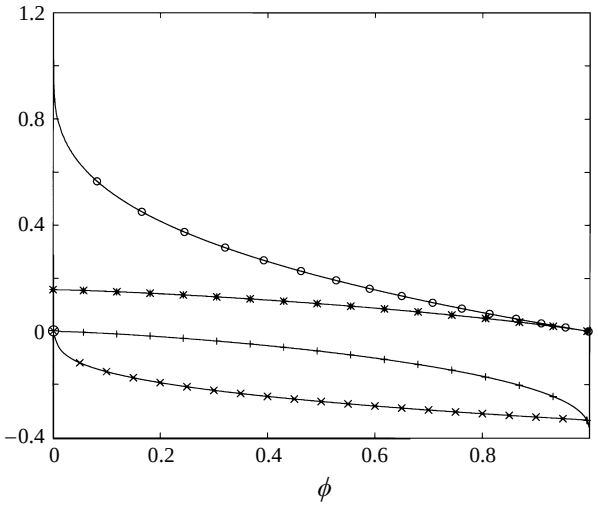

FIGURE 4. One-dimensional sensitivity functions. Ice volume sensitivity function to accumulation $V_a^s(\phi)$ (+) and rate factor $V_C^s(\phi)$ (∗) for the symmetric case and divide-position sensitivity function $K_a^a(0,\phi)$ (o) and $K_C^a(0,\phi)$ (x). Notice how sensitivity to accumulation occurs at the divide while sensitivity to the rate factor (and basal topography) is increased at the margin. For base case $v = 3, \delta = 4, \gamma = 7, d = 0$.

influence functions computed using Neuman series can be used, as comparison to equations (4.1) showed very small errors as described in §4.1.

Figures 3(*c*) and 5(*a*) show that the exponential ramp model (Nye 1959, Jóhannesson 1992) for flow down an infinite section is a good qualitative model of the Green's functions for sensitivity to rate-factor variation and bedrock forcing. Defining $\ell_1 \partial_x s_1 = -(s_1 - b_1)$ the perturbation problem along an infinite ramp has solution $s_1 = \int_{-\infty}^{\infty} g(x-\xi) b_1 \mathrm{d}\xi$ where the Green's function is

$$g(x-\xi) = \begin{cases} \dfrac{1}{\ell_1} \exp\left(\dfrac{x-\xi}{\ell_1}\right), & \xi < x \\ 0, & \xi > x, \end{cases}$$

the exponential ramp (Jóhannesson 1992). The increased sensitivity near the margin is qualitatively predictable from the infinite-slope model.

Figure 5(*b*), shows the influence function for antisymmetric response to rate-factor and bed variation. The influence represents a rate-factor forcing and the response represents the local coordinate stretching. A positive rate-factor forcing causes a negative divide deviation. This negative deviation of the coordinate is maintained until the line $\xi = \phi$, after which the deviation is positive. The physical interpretation of this is that upstream of the forcing, slopes are gentler while downstream, slopes are greater. A bump or a decrease in rate factor have the same effect.

We may compute the volume sensitivity kernel function V_C^s

$$V_C^s(\phi) = \int_0^1 K_C^s(\xi,\phi)\mathrm{d}\xi, \quad \int_0^1 \eta_1 \mathrm{d}\phi = \int_0^1 V_C(\phi) C_1 \mathrm{d}\phi,$$

which is also plotted in figure 4, showing that volume is most strongly dependent on rate-factor perturbations at the margin. The divide-position influence function $K_C^a(0,\phi)$ is also plotted in figure 4.

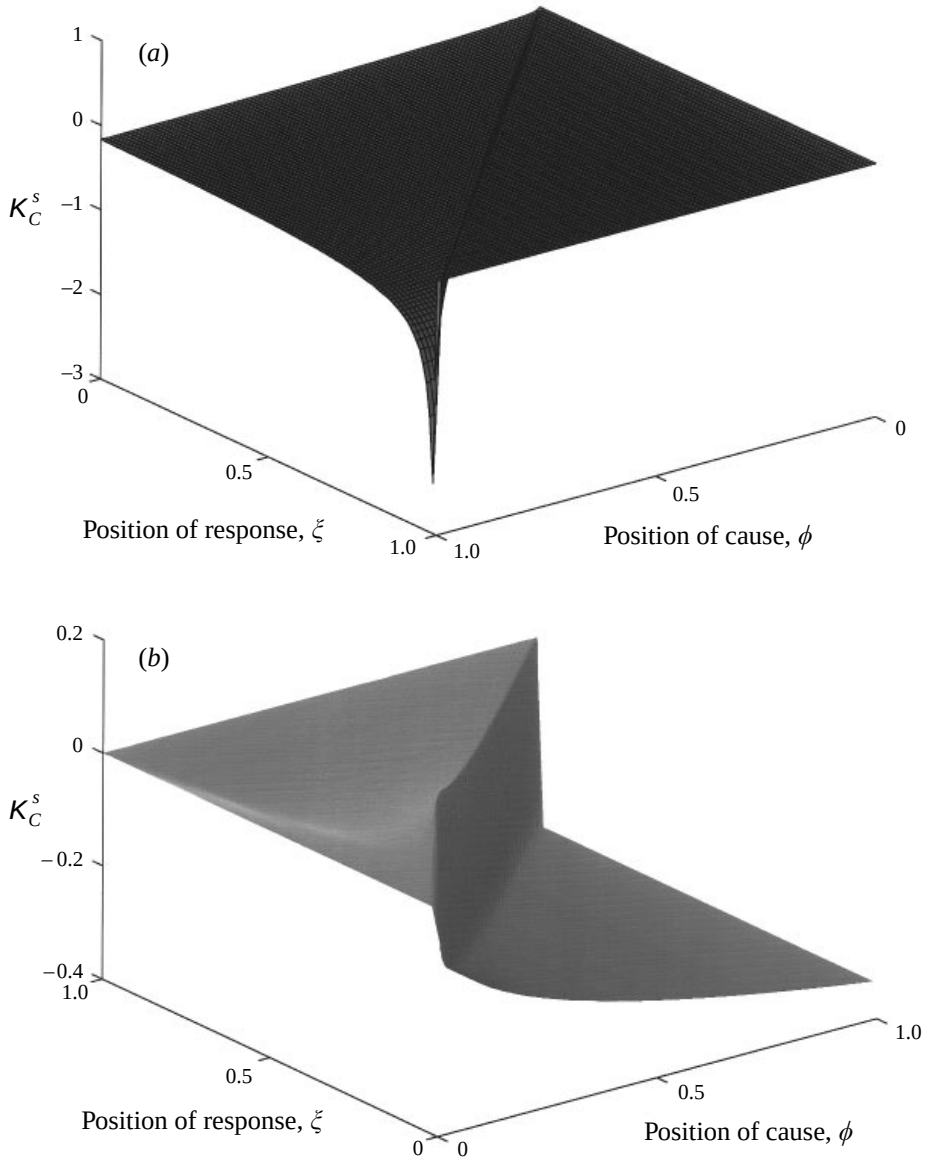

FIGURE 5. Rate factor/topography influence function (*a*) $K_C^s(\xi, \phi)$ for the symmetric base case and (*b*) $v = 3$, $\delta = 4$, $\gamma = 7$, $d = 0$. $K_C^a(\xi, \phi)$ for the antisymmetric base case.

4.3. *Time-dependent response*

A standard derivation (e.g. Hindmarsh 1996) shows that the accumulation distribution needed to excite mode i alone is given by $a_1 = (\mathscr{W}/\mathscr{S})\mathscr{E}_i$. The slowest decaying mode, $i = 1$, is plotted for symmetric and antisymmetric cases (figure 6). The sensitivity of the symmetric slow mode is greatest to accumulation rate variation in the centre of the ice sheet, similar to the steady response, while the transient sensitivity of the divide position is greatest halfway between divide and margin, different from the steady response.

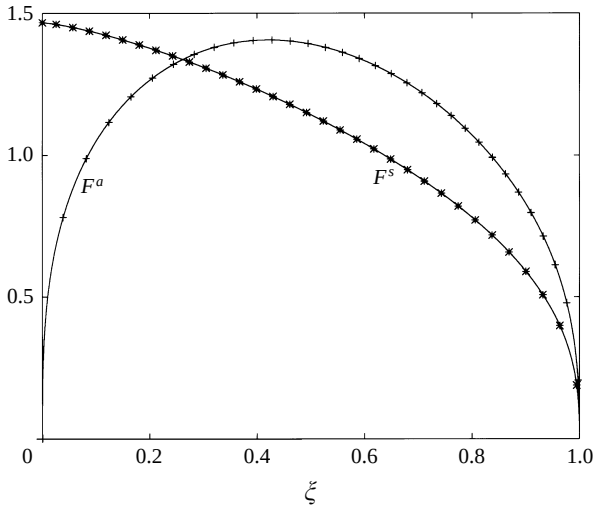

FIGURE 6. Accumulation rate distributions $\mathscr{F}^s(\xi), \mathscr{F}^a(\xi)$ which excite the slowest modes for symmetric forcing (*) and antisymmetric forcing (+), base case $v = 3$, $\delta = 4$, $\gamma = 7$, $d = 0$.

4.4. *A generalized VN solution*

We now generalize our models of the spatial dependence of C_0 to power-law forms, $C_0(\xi) = C_m |\xi|^r$, and introduce the bed multiplier $\beta_0(\xi) = \beta_m |\xi|^{f/m}$ which introduces zeroth-order basal topography through the construction

$$H_0 = s_0\beta, \quad b_0 = s_0 - H_0 = s_0(1 - \beta_0).$$

For positive indices this power-law construction implies that the rate factor and thickness vanish at the origin. These are not plausible physical descriptions, but may be considered as asymptotic cases where the rate factor and thickness become very small at the divide.

Extending the definitions $\alpha \equiv f + r$, $\delta \equiv v + 1 - \alpha$, $\delta_1 \equiv d - \alpha + 1$, we obtain

$$\eta_0(\xi) = \left(1 - |\xi|^{\delta/n}\right)^{n/(\gamma+1)}, \quad \frac{s_d^{\gamma+1}}{S^\delta} = \left(\frac{\gamma+1}{\delta}\right)^v \frac{a_m}{\beta_m^m C_m \delta_1},$$

which should be compared with the base-case VN solution (3.2). The profile is still a hyper-ellipse. Changing the flow geometry produces a small difference to the thickness for a given span (Nye 1959), and altering the other indices for rate factor, thickness etc. has a similarly muted effect.

We can use exactly the same symmetric perturbation equation with the above altered definitions of the parameters, provided we restrict consideration to $f = 0$. The construction is straightforward provided one notes that $H = \beta_0 s_0(1 + s_1/\beta_0)$. Defining also

$$\psi \equiv \frac{m/\beta + v}{\gamma + 1},$$

we obtain an eigenvalue problem

$$\partial_\xi\left(\xi^{d+2-\delta/v}\left(1 - \xi^{\delta/v}\right)^{1+\psi}\partial_\xi\eta_1\right) - \xi^d\left(1 - \xi^{\delta/v}\right)^\psi\left(\frac{\delta}{v}(d+1) + \lambda\eta_0\right)\eta_1 = 0.$$

The slowest-mode eigenvalues were calculated by shooting and are given in table 2.

β	1	1	1	1	0.5	1.5	0.5	1.5	0.5	1.5
d	0	0	1	0	0	0	1	1	0	0
α	0	−1	0	1	0	0	0	0	−1	−1
$-\lambda_1$	9.1	8.9	20	9.4	8.9	9.2	19	20	8.7	9.0

TABLE 2. Eigenvalues of slowest mode $-\lambda_1$ from the generalized symmetric perturbation. The parameter β is the thickness/elevation multiplier (unity in the base case), while longitudinal variation in properties is accounted for by the parameter α. The parameter d represents the dimension of the flow. See text for further explanation. $v = 3$, $\gamma = 7$ in all cases.

Having considered the effects due to variation of the flow geometry, the variation in the rate of relaxation of the slowest mode with basal topography is minimal and with the singular spatial variations in rate factor is small. Ice-sheet response is extremely robust to severe parameter ignorance. The results can be qualitatively explained by considering the low sensitivity of the zeroth-order profile (3.4) to changes in the parameters (see Figure 1). The perturbation equation (2.12) shows that by fixing the ice flux, the zeroth-order quantities only enter with unit exponents. Changing the zeroth-order profile does not significantly change the perturbation equation as the important control is the ice flux. This low sensitivity is of use in the following section.

4.5. *Normal-mode initialization*

Normal-mode expansions are used to project data onto certain modes with desirable properties (Daley 1991). One aim of initialization in ice-sheet models is to filter out the high-wavenumber variation in the surface topography. This variation is principally caused by high-wavenumber variation in the poorly known basal topography (Nye 1959).

Consider a measured ice-sheet profile $\hat{\eta}$. We wish to project it onto the zeroth-order solution and m linearized modes. Since the linear modes form a complete set, any residual from the zeroth-order solution can be projected onto them, implying that zeroth mode is non-unique. Let us write $\hat{\eta} = \eta_0(c^0 + \sum^{\infty} c_i^1 \mathscr{E}_i)$ where c_i^j are constants. We integrate over the domain and use the orthogonality relations to obtain

$$\int \mathscr{E}_i \mathscr{W}(\xi) \frac{\hat{\eta}}{\eta_0} \mathrm{d}\xi = c^0 \int \mathscr{E}_i \mathscr{W}(\xi)\, \mathrm{d}\xi + c_i^1, \quad i = 1, \infty.$$

We truncate and restrict consideration to m modes, writing $\hat{\eta} = c^0\eta_0 + \sum^m c_i^1 \mathscr{E}_i \eta_0 + \sigma\eta_0$ where σ is an error term, and after using the orthogonality relationships m times, arrive at

$$\int \mathscr{E}_i \mathscr{W}(\xi) \frac{\hat{\eta}}{\eta_0} \mathrm{d}\xi = c^0 \int \mathscr{E}_i \mathscr{W}(\xi)\, \mathrm{d}\xi + c_i^1 + c^0 \int \mathscr{E}_i \mathscr{W}(\xi)\, \sigma \mathrm{d}\xi, \quad i = 1, m.$$

Since the error term σ is the sum of the all the unconsidered modes orthogonal to the ith linear mode, the term involving the error is identically zero, and we are left with m equations involving $m + 1$ unknowns. Adding the m equations, squaring, minimizing the sum of the squares of the linear modes yields the following equation for the zeroth mode:

$$c^0 = \frac{\sum \int \mathscr{E}_i \mathscr{W}(\xi)\, \hat{\eta}/\eta_0 \mathrm{d}\xi}{\sum \int \mathscr{E}_i \mathscr{W}(\xi)\, \mathrm{d}\xi}.$$

This relationship is independent of the values of c_i^1.

5. Summary and further work

These calculations have informed us about the spatial variation in the sensitivity of ice-sheet response to perturbation in steady state and in transient response. Variations in accumulation forcing comparable with those experienced by some ice sheets during ice-age cycles produce a response sufficiently small to be describable by linearization techniques. Steady and symmetric response are more sensitive to accumulation rate variation in the centre of the ice sheet, while transient divide response is more sensitive to accumulation rate variation halfway between divide and margin. The sensitivity function can be regarded as an ideal sampling density function. Accumulation-rate measurements designed to constrain glaciological response should have a higher density in the central area of an ice sheet.

The use of these expansions for normal-mode initializations has been pointed out and a simple scheme outlined. The robustness of the perturbations to ignorance of the rheological properties of ice indicates that normal-mode initializations are practicable in the absence of precise knowledge of the ice rheology and can therefore be useful in short-term predictions.

I have had instructive conversations with Andrew Fowler, Kolumban Hutter, Tómas Jóhannesson, Elizabeth Morris, John Nye and John Pryce. I used a driver for SLEDGE written by Marco Marletta.

REFERENCES

Birkhoff, G. & Rota, G. C. 1989 *Ordinary Differential Equations*, 4th Edn. Wiley.

Bodvarsson, G. 1955 On the flow of ice sheets and glaciers. *Jökull* **5**, 1–8.

Courant, R. & Hilbert, D. 1953 *Mathematical Methods for Physicists*. Wiley.

Daley, R. 1991 *Atmospheric Data Analysis*. Cambridge University Press.

Fowler, A. C. 1992 Modelling the dynamics of ice sheets. *Geophys. Astrophys. Fluid Dyn.* **63**, 29–66.

Glen, J. W. 1955 The creep of poly-crystalline ice. *Proc. R. Soc. Lond.* A **226**, 519–538.

Halfar, P. 1981 On the dynamics of ice sheets. *J. Geophys. Res.* **86**, 11061–11072.

Hindmarsh, R. C. A. 1990 Time-scales and degrees of freedom in the evolution of continental ice-sheets. *Trans. R. Soc. Edinb. Earth Sci.* **81**, 371–84.

Hindmarsh, R. C. A. 1992 Estimating ice-sheet response to climate change. In *The Contribution of the Antarctic Peninsula to Sea-Level Rise* (ed. E. M. Morris). Report for the Commission of the European Communities Project, British Antarctic Survey, Cambridge.

Hindmarsh, R. C. A. 1996 Stochastic perturbation of divide position. *Ann. Glaciol.* **23**, 105–115.

Hutter, K. 1983 *Theoretical Glaciology*. Reidel.

Jóhannesson, T. 1992 The landscape of temperate ice caps. PhD Thesis, University of Washington.

Kreyszig, E. 1988 *Engineering Mathematics*, 6th Edn. Wiley.

Morland, L. W. 1984 Thermo-mechanical balances of ice sheet flows. *Geophys. Astrophys. Fluid Dyn.* **29**, 237–266.

Nagata, T. 1977 A Theoretical steady state profile of ice sheets (two-dimensional model). *Antarctic J.* **60**, 13–27.

Nye, J. F. 1952 A method of calculating the thickness of ice-sheets. *Nature* **169**, 529–530.

Nye, J. F. 1959 The motion of ice sheets and glaciers. *J. Glaciol.* **3**, 493–507.

Oerlemans, J. 1981 Effect of irregular fluctuations in antarctic precipitation on global sea level. *Nature* **290**, 770–772.

Pruess, S. & Fulton, C. T. 1993 Mathematical software for Sturm–Liouville problems. *ACM Trans. Math. Software* **19**, 360–376

Pryce, J. D. 1993 *The Numerical Solution of Sturm–Liouville Problems*. Oxford University Press.

Roach, G. 1982 *Green's Functions*, 2nd Edn. Cambridge University Press.

SZIDAROVSKY, F., HUTTER, K. & YAKOWITZ, S. 1986 Computational ice-divide analysisof a cold plane ice-sheet under steady conditions. *Ann. Glaciol.* **12**, 170–177.

VAN DER VEEN, C. J. 1993 Interpretation of short-term elevation changes inferred from satellite altimetry. *Climatic Change* **23**, 383–406.

VIALOV, S. S. 1958 Regularities of ice deformation. In *International Association of Scientific Hydrology 47, Symposium at Chamonix 1958 - Physics of the Movement of Ice*, pp. 383–391.

WEERTMAN, J. 1961 Equilibrium profile of ice caps. *J. Glaciol.* **3**, 953–964.

WEERTMAN, J. 1973 Position of ice divides and ice centers on ice sheets. *J. Glaciol.* **12**, 353–360.